Direct numerical simulations of bubble-laden turbulent flows using the two-fluid formulation

O. A. Druzhinin, and S. Elghobashi

Citation: Physics of Fluids **10**, 685 (1998); doi: 10.1063/1.869594
View online: https://doi.org/10.1063/1.869594
View Table of Contents: http://aip.scitation.org/toc/phf/10/3
Published by the American Institute of Physics

Direct numerical simulations of bubble-laden turbulent flows using the two-fluid formulation

O. A. Druzhinin[a] and S. Elghobashi
Department of Mechanical and Aerospace Engineering, University of California, Irvine, California 92697

(Received 12 August 1997; accepted 25 November 1997)

Direct numerical simulations (DNS) of bubble-laden isotropic decaying turbulence are performed using the two-fluid approach (TF) instead of the Eulerian–Lagrangian approach (EL). The motivation for the study is that EL requires considerable computational resources, especially for the case of two-way coupling, where the instantaneous trajectories of a large number of individual bubbles need to be computed. The TF formulation is developed by spatially averaging the instantaneous equations of the carrier flow and bubble phase over a scale of the order of the Kolmogorov length scale, which, in our case, is much larger than the bubble diameter. On that scale, the bubbles are treated as a continuum (without molecular diffusivity) characterized by the bubble phase velocity field and concentration (volume fraction). The bubble concentration, C, is assumed small enough ($C \leqslant 10^{-3}$) to neglect the bubble–bubble interactions. As a test case, direct simulation of a bubble-laden Taylor–Green vortex with one-way coupling is performed with a bubble response time of the order of the flow time scale (inverse of the mean vorticity). This simple flow allows a direct examination of the effects of the preferential accumulation of bubbles in the high-enstrophy regions of the flow on the accuracy of the two-fluid formulation. The temporal development of the maximum bubble concentration obtained from DNS agrees well with the analytical solution. DNS of the bubble-laden decaying turbulence are also performed for both cases of one-way and two-way coupling. Here, the bubble diameter and response time are much smaller than the Kolmogorov length and time scales, respectively. In this case, as expected, the effects of the preferential accumulation of the bubbles are not pronounced. The results also show that the bubble-laden flow is analogous to a stratified flow with an effective density $=(1-C)\rho_f$. Thus, due to the two-way interaction between the bubbles and carrier flow, the turbulence decay is enhanced with stable stratification, and reduced with unstable stratification. © *1998 American Institute of Physics.* [S1070-6631(98)02203-X]

I. INTRODUCTION

All published DNS studies of turbulent flows laden with particles adopt the Lagrangian–Eulerian approach. In this approach the carrier flow velocity field is obtained by solving the Navier–Stokes and continuity equations at fixed mesh points, whereas the trajectories of the dispersed particles are computed by solving the Lagrangian equation of particle motion.[1,2] Employing this method to simulate turbulent flows with two-way coupling between the particles and the carrier flow is limited at present and in the foreseeable future by the memory and speed of available supercomputers (including the latest parallel supercomputers). For example, for spherical particles with 50 μ diameter and occupying a volume fraction $\phi = 10^{-3}$, we need about 10^5 particles per cm^3, or millions of particles in a typical volume for a practical application. This fact together with computer limitations forces all DNS of particle-laden turbulent flows (with two-way coupling) to compute the trajectories of *only* a fraction of the *actual number* of particles. The accuracy of DNS results is directly proportional to the magnitude of this fraction, being highest when the fraction equals unity.[2]

The alternative approach for predicting particle-laden flows is known as the ''two-fluid,'' or ''Eulerian–Eulerian,'' approach,[3] and has been employed only with the Reynolds-averaged equations of motion, not with DNS. In this approach, the governing equations are obtained by volume averaging the equations of motion of both phases (the carrier flow and particles) based on the assumption that the dispersed particles behave as a ''continuum'' under certain conditions. In predicting practical dispersed two-phase flows using the two-fluid approach, time averaging is performed on the volume-averaged equations of motion, thus resulting in the closure problem, where second- and higher-order correlations of both phases need to be modeled.

The objective of this paper is to describe how DNS can be performed using the two-fluid approach for bubble-laden homogeneous isotropic turbulence without forcing (i.e., decaying turbulence).

It is important to point out that in employing the two-fluid approach a difficulty may arise due to the phenomenon of preferential accumulation of the dispersed particles. It is well known[4] that solid particles, due to their inertia, tend to

[a]On leave from the Applied Physics Institute, Russian Academy of Sciences, 603600 Nizhni Novgorod, Russia.

accumulate in the low-enstrophy regions of the flow, whereas gaseous bubbles in a liquid flow tend to accumulate in high-enstrophy regions, generally associated with the centers of vortices. Preferential accumulation in homogeneous turbulence is most pronounced for particles with response times of the order of the Kolmogorov time scale τ_k.[5] This segregation creates regions devoid of particles neighboring regions of high particle concentration. Therefore, performing DNS using the two-fluid approach may generate large concentration gradients causing numerical resolution and stability problems, thus restricting the implementation of that approach.

In this paper we show that the two-fluid approach is applicable to bubbles with diameter smaller than the Kolmogorov length scale, and accordingly their response time is much smaller than the Kolmogorov time scale. Thus, the effects of preferential accumulation of bubbles in the high-enstrophy regions of the carrier flow become less pronounced, so that DNS with the two-fluid approach can be successfully used.

Turbulent liquid flows laden with gaseous bubbles whose diameter is smaller than the Kolmogorov length scale exist in nature (bubbles in the wakes of ships in the ocean) and in chemical processing industries. A recent laboratory experiment by Rightley (1995)[6,7] provides an example of such flows. In that experiment, a turbulent bubble-laden mixing layer was created, with momentum thickness 5 mm$\leqslant\delta\leqslant$40 mm and fluid rms velocity 0.03 m/s$\leqslant u_{\rm rms}\leqslant$0.05 m/s. Microbubbles were generated with free-stream volume fraction $\alpha=1.5\times10^{-5}$ and diameters in the range 20 μm $\leqslant d_b\leqslant$100 μm, which are smaller than the Kolmogorov length scale, η, estimated as $\eta\simeq$400 μm (for liquid water viscosity $\nu=10^{-6}$ m^2/s).

The paper is organized as follows. In Sec. II the governing equations of motion of the bubble-laden flow and the numerical method are described. The results for the bubble-laden Taylor–Green vortex and isotropic decaying turbulence with one-way coupling are presented in Sec. III. The effects of the two-way coupling on isotropic turbulence are discussed in Sec. IV. Concluding remarks are presented in Sec. V.

II. GOVERNING EQUATIONS AND NUMERICAL METHOD

A. Equations of motion for the bubble-laden flow

We consider spherical bubbles with diameter d much smaller than the characteristic length scale of the flow, L_f, and average the equations of motion of the fluid and bubble over a length scale scale λ that is much smaller than L_f but much larger than the bubble diameter, $d\ll\lambda\ll L_f$. Thus the bubble phase can be treated as a continuum characterized by the velocity $V_i(\mathbf{r},t)$ and concentration (or volume fraction) $C(\mathbf{r},t)=\pi d^3 n(\mathbf{r},t)/6$, where $n(\mathbf{r},t)$ is the bubble number density.

We assume that the density of the gas and, consequently, the mass of the bubble are negligible compared to those of the surrounding fluid, $\rho_f\gg\rho_b=0$. Taking into account the effect of the bubbles on the fluid flow in a unit volume of the mixture and neglecting the interactions between the bubbles, we write the following equations for the bubble-laden flow:[8,9] (a) the fluid momentum equation,

$$(1-C)\rho_f\frac{DU_i}{Dt}=-(1-C)\partial_i P+\partial_j(1-C)\sigma_{ij}-CF_i^d-(1-C)\rho_f g\,\delta_{iz}; \tag{1}$$

(b) the fluid continuity equation,

$$-\partial_t C+\partial_j(1-C)U_j=0; \tag{2}$$

(c) the bubble-phase momentum equation,

$$0=-C\partial_i p+\partial_j C\sigma_{ij}+CF_i^d; \tag{3}$$

(d) the bubble-phase continuity equation,

$$\partial_t C+\partial_j CV_j=0. \tag{4}$$

In the above equations, U_i is the fluid velocity, V_i is the velocity of the bubble phase, σ_{ij} is the viscous stress tensor, $\sigma_{ij}=\mu(\partial_j U_i+\partial_i U_j)$, the Lagrangian derivatives $D/Dt=\partial/\partial t+U_j\partial_j$ and $d/dt=\partial/\partial t+V_j\partial_j$ are taken along the trajectories of the fluid point and bubble, respectively, and g is the projection of the gravity acceleration on the z axis, $g_i=-g\,\delta_{iz}$. Here F_i^d denotes the force acting on the bubble due to the pressure and viscous stresses caused by the disturbance flow U^d, owing to the boundary conditions at the bubble surface. The details of the derivation of Eqs. (3)–(4) are given in the Appendix.

Since we assume that the bubble mass is negligible, the sum of the forces acting on the bubble must vanish, and thus the equation of the bubble motion becomes

$$F_i^0+F_i^d=0, \tag{5}$$

where F_i^0, the force exerted on the bubble by the undisturbed fluid flow U^0, is obtained by integrating both the pressure and viscous stresses of the undisturbed flow over the bubble surface. For small spherical bubbles with diameter much smaller than the flow length scale,

$$d_b\ll L_f, \tag{6}$$

and with Weber number less than unity, F_i^0 is given by

$$F_i^0=\rho_f\left(\frac{DU_i^0}{Dt}+g\,\delta_{iz}\right)=-\partial_i P^0+\partial_j\sigma_{ij}^0, \tag{7}$$

where P^0 and σ_{ij}^0 are the undisturbed pressure and viscous stresses fields, respectively (cf. the Appendix).

The prescription of the boundary conditions at the surface of a spherical bubble depends mainly on the properties of the surrounding liquid and the bubble Reynolds number. Available experimental data[10–13] for a bubble rising in a stagnant nonpurified liquid water with Reynolds number less than unity show that the drag force on the bubble, D, is described by the Stokes law, $D=3\pi d_b\rho_f\nu W$ (where W is the bubble terminal velocity), rather than by the Hadamard–Rybczynski formula, $D=2\pi d_b\rho_f\nu W$. The reason is that in a nonpurified water, the gas–liquid interface is ''solidified,'' owing to the presence of impurities. Thus, the boundary condition at the bubble surface is effectively equivalent to that

for a solid sphere rather than the free-stress condition needed for the Hadamard–Rybczynski formula.[11] Thus, for bubbles with Reynolds number less than unity,

$$\mathrm{Re}_b=\frac{d_b|U^0-V|}{\nu}<1, \tag{8}$$

the force due to the disturbance flow, F^d, can be calculated from the solution of the corresponding unsteady Stokes problem in the form

$$F_i^d=\frac{18\mu}{d^2}(U_i^0-V_i)+\frac{\rho_f}{2}\left(\frac{DU_i^0}{Dt}-\frac{dV_i}{dt}\right). \tag{9}$$

The first and second terms in (9) correspond to the Stokes drag and added-mass forces, respectively. In the considered case of a small bubble, the Basset and lift forces can be neglected. The recent theoretical studies[14,15] show that the influence of the Basset force is negligible due to the enhanced temporal decay of the integral kernel. Also, the experimental measurements by Sridhar and Katz[16] for bubbles with diameters 500 μm$<d_b<$800 μm show that the effect of the Basset force is negligible compared to that of the drag and lift forces. In addition, Maxey and Riley[17] show analytically that the lift force on a microparticle is negligible. Therefore, we neglected the Basset and lift forces in the case of microbubbles.

We obtain from Eq. (5) an equivalent expression for the disturbance force:

$$F_i^d=-F_i^0, \tag{10}$$

where F_i^0 is given by (7).

Therefore, the equation of the bubble motion (5) can be rewritten in the form

$$\frac{dV_i}{dt}=3\frac{DU_i}{Dt}+\frac{1}{\tau_b}(U_i-V_i+W\delta_{iz}), \tag{11}$$

where the bubble response time τ_b and terminal velocity W are defined as

$$\tau_b=\frac{d^2}{36\nu}, \tag{12}$$

and

$$W=2\tau_b g. \tag{13}$$

In Eqs. (1)–(4), (11), and the following discussion we omit the superscript ''0'' in the notation for the undisturbed flow U^0.

We assume that the bubble concentration, C, is small enough (i.e., $C\leqslant 10^{-3}$), and thus neglect its contribution to the fluid inertia and continuity, i.e., we retain C only in the buoyancy term in the momentum equation of the carrier flow (1). This is analogous to the Boussinesq approximation in a stratified fluid with effective density $(1-C)\rho_f$.

Substituting the expression for the disturbance force obtained from Eqs. (10) and (7) into the equation for the fluid momentum (1), and using (11), we write equations of the conservation of the fluid and bubble phase momentum and mass in the form[18]

$$\frac{DU_i}{Dt}=-\frac{1}{\rho_f}\partial_i\tilde{P}+\nu\Delta U_i+(C-\langle C\rangle)g\delta_{iz}, \tag{14}$$

$$\partial_j U_j=0, \tag{15}$$

$$\frac{dV_i}{dt}=3\frac{DU_i}{Dt}+\frac{1}{\tau_b}(U_i-V_i+W\delta_{iz}), \tag{16}$$

$$\frac{\partial C}{\partial t}+\partial_j CV_j=0. \tag{17}$$

Using the analogy between the bubbly flow and a stratified flow with density $(1-C)\rho_f$, we remove the modified hydrostatic part in the pressure field in Eq. (14),

$$\tilde{P}=P+\rho_f g\int_0^z(1-\langle C\rangle)dz, \tag{18}$$

where $\langle C\rangle$ is the ensemble-averaged bubble concentration. In the following discussion, we evaluate $\langle C\rangle$ as an average over a horizontal (z) plane.

B. Numerical method

The momentum conservation and continuity equations (14)–(17) for both phases are solved in a cubical domain with periodic boundary conditions. The equations are discretized in an Eulerian framework using a second-order finite-difference technique on a staggered grid containing 96^3 points equispaced within unit length in each of three coordinate directions (x,y,z). The Adams–Bashforth scheme is used to integrate the equations in time. Pressure is obtained by solving the Poisson equation using Fast Fourier Transform. More details about the numerical method and its accuracy are discussed by Elghobashi and Truesdell,[19] Gerz *et al.*,[20] and Schumann.[21]

We perform the DNS for two different flows: the Taylor–Green (TG) vortex and the decaying isotropic turbulence. The TG flow field is discussed in detail in Sec. III. In the case of decaying turbulence, we use an initialization algorithm to generate a divergence-free random fluid velocity field with a prescribed energy spectrum $E(k)$ and spectral cross-correlations matrix $R_{ij}(k)$ of the velocity and scalar concentration, satisfying the realizability constraints.[21] The initial energy spectrum is prescribed by

$$E(k,0)=\frac{3u_0^2}{4\pi}\frac{k}{k_p^2}\exp\left(-\frac{k}{k_p}\right), \tag{19}$$

where u_0 is the dimensionless rms velocity, $k=1,\ldots,N_g/2$ is the wave number for the given grid resolution ($N_g=96$), and k_p is the wave number of peak energy. The wave number is normalized by the lowest nonzero wave number $k_{\min}=2\pi$. The dimensionless kinematic viscosity ν is calculated from the prescribed initial microscale Reynolds number $\mathrm{Re}_{\lambda 0}$ and the computed initial dissipation $\epsilon(0)$.

III. RESULTS

In this section we present the DNS results for bubble dispersion in a TG vortex with one-way coupling and isotropic decaying turbulence with both one-way and two-way coupling.

A. Dispersion of bubbles in a Taylor–Green vortex

Here we study the dispersion of small spherical bubbles in a Taylor–Green vortex flow with one-way coupling. The main objective of this test case is to examine the effects of the preferential accumulation of bubbles in this flow on the performance of the numerical method with the two-fluid approach.

This flow represents an exact two-dimensional time-dependent solution of the Navier–Stokes equations[22] with velocity components $(U_x, U_y, 0)$. The corresponding instantaneous, local streamfunction can be written as

$$\Psi(x,y,t)=\frac{\omega_0}{k^2}\exp(-\nu k^2 t)\cos k_x x \cos k_y y, \tag{20}$$

where ω_0 is the initial vorticity maximum, k_x and k_y are the wave numbers in x and y directions, and $k^2=k_x^2+k_y^2$. The flow vorticity, ω, and pressure, P, are

$$\omega=\frac{\partial U_y}{\partial x}-\frac{\partial U_x}{\partial y}=k^2\Psi, \tag{21}$$

$$P=P_0-\frac{1}{2}\left[\left(\frac{\partial \Psi}{\partial x}\right)^2+\left(\frac{\partial \Psi}{\partial y}\right)^2+k^2\Psi^2\right]. \tag{22}$$

The fluid velocity components are

$$U_x=\frac{\partial \Psi}{\partial y}=-\omega_0\frac{k_y}{k^2}\exp(-\nu k^2 t)\cos\, k_x x\, \sin\, k_y y, \tag{23}$$

$$U_y=-\frac{\partial \Psi}{\partial x}=\omega_0\frac{k_x}{k^2}\exp(-\nu k^2 t)\sin\, k_x x\, \cos\, k_y y. \tag{24}$$

We assume that the gravitational acceleration is normal to the flow plane (x,y), so that it does not affect the bubble dynamics on that plane.

The computations are performed for a flow Reynolds number $\mathrm{Re}=1/\nu=5000$ and an initially uniform concentration (volume fraction) of bubbles with response time $\tau_b=0.25$. We set the parameters $k_x=k_y=2\pi$ and $\omega_0=1$. The initial fluid velocity and pressure are prescribed by Eqs. (22), (23), and (24) at $t=0$. The initial horizontal velocity components V_x and V_y of the bubble are set equal to zero,

$$V_x=0, \quad V_y=0. \tag{25}$$

The initial bubble concentration is a uniform constant, $C_0=\alpha_0$, where the reference bubble volume fraction α_0 is assumed to be sufficiently small to neglect the influence of the bubble on the carrier flow (i.e., only one-way coupling is considered).

The direct simulation is performed with a mesh of $(96)^3$ points and continued for dimensionless time $0\leqslant t\leqslant 14$. Although the TG-vortex flow studied here is essentially two dimensional, the numerical method uses a three-dimensional (3D) algorithm, and the flow is homogeneous in the z direction.

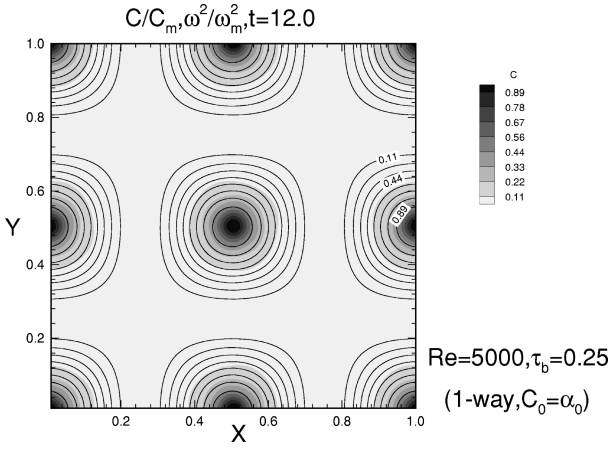

FIG. 1. Enstrophy and bubble concentration normalized by the maximum values. (The increment for the enstrophy isolines is equal to the increment in the table for the bubble concentration.)

Figure 1 shows the contours of the enstrophy, ω^2, and bubble concentration, C (in the gray scale) in the (x,y) plane at $z=0.5$ and time $t=12$. The figure shows that the bubbles accumulate, and sharp peaks of the concentration are formed at the vortex centers located at points $(x=0,\ y=0)$ and $(x=0.5,\ y=0.5)$, corresponding to the local maxima of the enstrophy.

In order to quantify the accumulation effects and the correlation between the flow enstrophy and bubble concentration, we calculate the average concentration and its variance conditioned on the magnitude of enstrophy, $\langle C\rangle_\omega$ and $\langle C'^2\rangle_\omega$, defined as

$$\langle C\rangle_\omega=\frac{1}{N(\omega^2)}\sum_{j=1}^{N(\omega^2)} C_j/C_0, \tag{26}$$

$$\langle C'^2\rangle_\omega=\frac{1}{N(\omega^2)}\sum_{j=1}^{N(\omega^2)} (C_j/C_0-\langle C\rangle_\omega)^2, \tag{27}$$

where $N(\omega^2)$ is the number of grid points where the enstrophy value lies within the range $[\omega^2,\omega^2+\Delta\omega^2]$, where $\Delta\omega^2=0.025$. Figure 2 shows the dependence of $\langle C\rangle_\omega$ and $\langle C'^2\rangle_\omega$ on the enstrophy of the flow displayed in Fig. 1. As expected,[23,24] both the bubble concentration and its variance increase with increasing ω^2. The growth of $\langle C'^2\rangle_\omega$ is caused by the preferential accumulation of bubbles in a smaller number of computational cells [see Eq. (27)].

The growth of the bubble concentration at the vortex centers can be described analytically, provided that the bubble response time is small compared to the flow time scale, i.e., $\tau_b<\tau_f$. The flow time scale, τ_f, in the case considered here is of the order $1/\omega_0\sim 1$. In this case, an approximate solution of Eq. (16) for the bubble velocity can be written in the form[25,26]

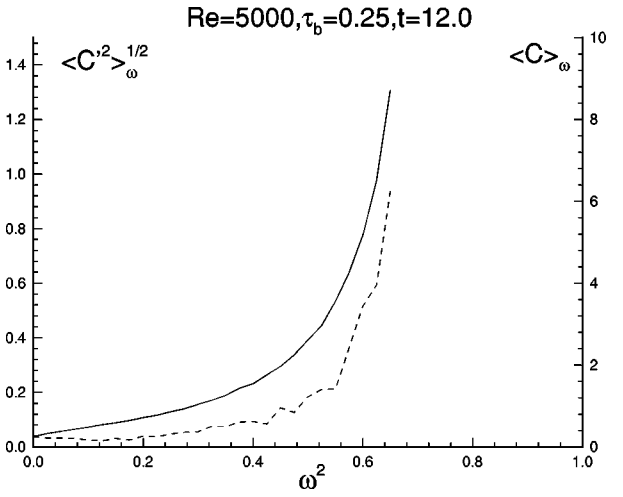

FIG. 2. Dependence of the enstrophy-conditioned average bubble concentration (solid curve) and its variance (dashed curve) on the flow enstrophy.

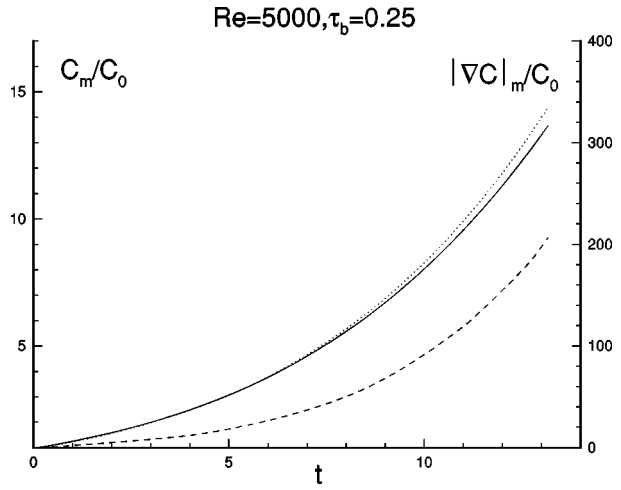

FIG. 3. Time dependence of the maximum bubble concentration and the modulus of the concentration gradient in the Taylor–Green vortex (full and dashed curves, respectively). The dotted curve corresponds to the analytical solution (33) for the concentration.

$$V_x = U_x + 2\tau_b \frac{DU_x}{Dt} + O(\omega_0^2 \tau_b^2),$$
$$V_y = U_y + 2\tau_b \frac{DU_y}{Dt} + O(\omega_0^2 \tau_b^2), \tag{28}$$

where $D/Dt = \partial_t + U_x \partial_x + U_y \partial_y$ and $\omega_0^2 \tau_b^2 = 1/16 \ll 1$. The dynamics of the bubble concentration is then described by the equation

$$\frac{DC}{Dt} = -2\tau_b \left[\frac{\partial}{\partial x}\left(C \frac{DU_x}{Dt} \right) + \frac{\partial}{\partial y}\left(C \frac{DU_y}{Dt} \right) \right]. \tag{29}$$

In the vicinity of the vortex center ($x_e = 0$, $y_e = 0$), corresponding to the elliptic stagnation point, the fluid velocity field corresponds to that of a decaying ''solid'' vortex, and the velocity components in the x and y directions are

$$U_x^e \simeq -\omega_0 \frac{k_y^2 y}{k^2} \exp(-\nu k^2 t), \tag{30}$$

$$U_y^e \simeq \omega_0 \frac{k_x^2 x}{k^2} \exp(-\nu k^2 t), \tag{31}$$

for $|x| \ll 1$, $|y| \ll 1$. Thus, the solution (28) for the bubble velocity can be recast as

$$V_x^e \simeq U_x^e - 2\tau_b \omega_0^2 x \frac{k_x^2 k_y^2}{k^4} \exp(-2\nu k^2 t),$$
$$V_y^e \simeq U_y^e - 2\tau_b \omega_0^2 y \frac{k_x^2 k_y^2}{k^4} \exp(-2\nu k^2 t). \tag{32}$$

The first terms in Eqs. (32) are the fluid velocity components, $U_{x,y}^e$, associated with the solid vortex rotation and thus contribute to the corresponding rotation of the bubble. The second terms represent the first-order correction caused by the inertia of the bubble, owing to the added mass, and describe the radial drift of the bubble toward the vortex center. This drift is caused by the pressure gradient force, directed toward the vortex center, which, for a bubble, is not balanced by the centrifugal force.

Now, the solution for the maximum bubble concentration, i.e., at the vortex center, C_m, for an initially uniform C_0 is obtained using (29) and (32) in the form

$$C_m = C_0 \exp\left[\frac{2\tau_b}{\nu} \left(\omega_0 \frac{k_x k_y}{k^3} \right)^2 [1 - \exp(-2\nu k^2 t)] \right]. \tag{33}$$

Figure 3 compares the time evolution of the maximum bubble concentration, i.e., at the vortex center, normalized by the initial concentration C_0, obtained from the analytical solution (33) (dotted line) with that of DNS (solid line) at ($x = 0.5$, $y = 0.5$). The agreement is excellent up to $t = 8$, after which a small difference occurs due to the continuous growth of the concentration gradient.

The figure also shows the time dependence of the maximum modulus of the concentration gradient (a dashed curve). The computations are performed until time $t = 14$, when $|\nabla C|_m / C_0 \simeq 200$. It should be noted that this time is equivalent to nearly 14 times the eddy turnover time of the flow considered. Continuation of the simulation beyond this time results in numerical instabilities due to the development of large concentration gradients.

In order to estimate a critical value of the local concentration gradient we consider the following condition for the smoothness of the bubble concentration field:

$$\frac{|\nabla C|}{C_0} \Delta x \ll 1, \tag{34}$$

where Δx is the grid cell size ($\Delta x = 1/N_g$) and C is a local concentration. Then the critical gradient $|\nabla C|_{\mathrm{cr}}$ is given by

$$\frac{|\nabla C|_{\mathrm{cr}}}{C_0} \sim \Delta x^{-1}. \tag{35}$$

In our DNS at $t=14$ we find the critical value of the concentration gradient $|\nabla C|_{\text{num}}/C_0 \sim O(10^2)$ (cf. Fig. 3) which is of the order of Δx^{-1} for the given grid resolution ($N_g=96$).

Note that in spite of the large value of the concentration gradient for times $5<t<14$, there is a good agreement between the analytical solution for the maximum concentration (33) and the numerical results (Fig. 3), indicating that numerical diffusion effects remain negligible.

Therefore, the results of this test case show that it is possible to use the two-fluid approach for the flow conditions, where the effects of preferential accumulation are resolved appropriately.

Note that in the considered test case, the bubble response time ($\tau_b=0.25$) is of the order of the flow time scale ($\tau_f=1$), and the effects of bubble accumulation are pronounced. In the next section we study the dispersion of bubbles in a decaying isotropic turbulence, assuming that the bubble diameter is much smaller than the Kolmogorov length scale. In this case, the bubble response time is much smaller than the Kolmogorov time scale, and the effects of the preferential accumulation are not pronounced.

B. Dispersion of bubbles in isotropic decaying turbulence (with one-way coupling)

DNS of bubble dispersion in isotropic decaying turbulence is performed with the following initial conditions: $\text{Re}_{\lambda 0}=25$, $u_0=0.05$, and $k_p/k_{\min}=5$, which correspond to the initial dissipation $\epsilon(0)=0.002\,584$, Taylor microscale $\lambda_0=0.027\,877$, Kolmogorov length scale $\eta_0=0.002\,861$, integral length scale $L_0=0.057\,815$, and viscosity $\nu=5.57\times10^{-5}$. The dimensionless gravity constant g is considered equal to unity. The reference length and time scales used in normalizing the above dimensionless quantities are $L_{\text{ref}}=0.098$ m and $T_{\text{ref}}=0.1$ s, respectively.

The initial bubble velocity and concentration are prescribed as

$$V_i=\delta_{iz}W, \quad C_0=\alpha_0, \tag{36}$$

where the bubble terminal velocity W is given by (13).

The ability of the simulation to resolve the motion at the smallest turbulence scales is assured by the criterion $\eta k_{\max}>1$, where $k_{\max}=N_g\pi$ is the highest resolved wave number for the given number of grid points in each coordinate direction N_g ($=96$ in the present case). Our simulations show that $1\leqslant \eta k_{\max}\leqslant 2.65$ for $0.75<t<10$.

The choice of the bubble response time is restricted by the conditions (6) and (8), which can be rewritten in the form

$$d_b<\eta, \tag{37}$$

and

$$\text{Re}_b=\frac{Wd_b}{\nu}<1. \tag{38}$$

The first condition ensures that the bubble size is smaller than the characteristic flow scale, i.e., the Kolmogorov length scale $\eta=(\nu^3/\epsilon)^{1/4}$ in the case of decaying isotropic turbulence. The second condition restricts the bubble Reynolds number, based on the bubble terminal velocity, to be less than 1. Substituting the terminal velocity (13) and the bubble diameter $[d_b=(36\nu\tau_b)^{1/2}]$ in (37) and (38), and using the equality $\eta^2=\nu\tau_k$, we rewrite the conditions (37) and (38), respectively, as

$$\frac{\tau_b}{\tau_k}<\frac{1}{36}\simeq 0.028, \tag{39}$$

and

$$\tau_b<\left(\frac{\nu}{144g^2}\right)^{1/3}=\tau_*. \tag{40}$$

It should be emphasized that the conditions (39) and (40) are essential for the derivation of the bubble motion equation (11). Thus, violating either of these conditions renders the equation of motion (11) invalid. Note that Wang and Maxey[23] and Maxey *et al.*[24] performed DNS of isotropic turbulence laden with bubbles with $\tau_b=\tau_k$ using the Eulerian–Lagrangian approach and Eq. (11), i.e., violating the condition (39).

Note also that in the case of solid particles, the condition $d_p<\eta$ (which is also required for the derivation of the particle motion equation) is equivalent to $(\tau_p/\tau_k)<(\rho_p/18\rho_f)$, which allows (τ_p/τ_k) to be $\geqslant 1$ for $\rho_p>18\rho_f$.

In our DNS of bubble-laden decaying turbulence we prescribe $\tau_b=0.04\tau_{k0}$, where the initial dimensionless Kolmogorov time scale is $\tau_{k0}=0.15$. The bubbles are added to the flow at time t=1, when the magnitude of the skewness of the fluid velocity derivative reaches about 0.47, indicating an established rate of energy transfer across the energy spectrum. At that time, τ_k increases to 0.22, so that ratio $\tau_b/\tau_k=0.027$ and the time $\tau_*=0.0073$ [see Eq. (40)]. Since τ_k increases monotonically in decaying turbulence, the condition (39) is satisfied throughout the simulation. Thus, both conditions (39) and (40) are met for the prescribed value of τ_b. The corresponding bubble Reynolds number (38) equals 0.74 (i.e., of the order of unity) and the dimensional bubble diameter is $d_b\simeq 350\mu$m (for the bubble to remain spherical in liquid water, i.e., d_b is less than 1 mm). Therefore, the prescribed value of τ_b is close to the maximum limit for the validity of the equation set (14)–(17).

Figure 4 shows the time development of the turbulence kinetic energy $E(t)$ and its dissipation rate $\epsilon(t)$ and the concentration variance $\langle C'^2\rangle=\langle (C-\langle C\rangle)^2\rangle$ calculated from the corresponding spectra $E(k,t)$ and $E_C(k,t)$ as

$$E(t)=\sum_{k=1}^{N_g/2} E(k,t), \tag{41}$$

$$\epsilon(t)=2\nu\sum_{k=1}^{N_g/2} k^2E(k,t), \tag{42}$$

and

$$\langle C'^2\rangle(t)=\sum_{k=1}^{N_g/2} E_C(k,t), \tag{43}$$

and normalized by the respective initial values $E(0)$, $\epsilon(0)$, and C_0^2. Both $E(t)$ and $\epsilon(t)$ decay in time due to the viscous dissipation. On the other hand, the bubbles concentration

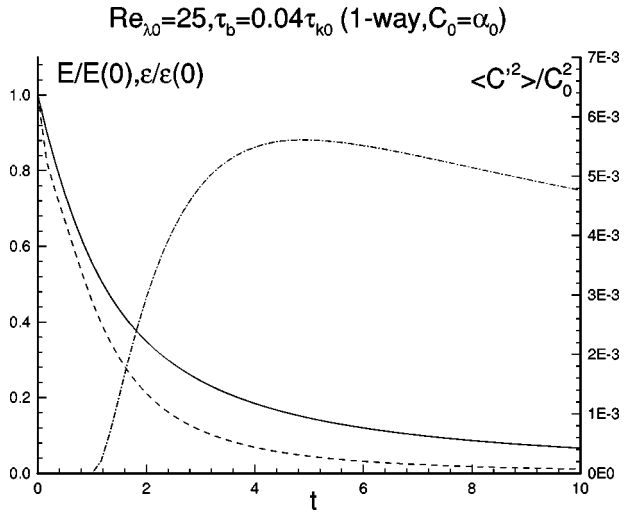

FIG. 4. The time dependence of the normalized turbulence kinetic energy $E(t)/E(0)$ (solid curve), its dissipation rate $\epsilon(t)/\epsilon(0)$ (dashed curve), and bubble concentration variance $\langle C'^2\rangle/C_0^2$ (dash–dotted curve).

variance first increases from zero to $\langle C'^2\rangle \simeq 5.1\times 10^{-3} C_0^2$ (for time $1<t<5$, where $t=1$ is the time of injecting the bubbles into the flow), and then decays. The growth of the concentration variance is caused by the preferential accumulation of bubbles in the high-enstrophy regions of the flow. The effects of the bubble accumulation, as well as the decay of the concentration variance for $t>5$, are discussed below.

Figure 5 shows the spectra of the fluid kinetic energy, $E(k)$, the dissipation, $\epsilon(k)=2\nu k^2 E(k)$, and the bubble concentration fluctuations, $E_C(k)$ at time $t=3$ [here and below, for convenience, we omit the explicit reference to the time dependence of $E(k,t)$, $\epsilon(k,t)$, and $E_C(k,t)$]. At this time, the energy spectrum peaks at $k=3$. Note that since the transport equation of bubble concentration is of the advection (Lagrangian) type, there is no molecular dissipation of the bubble concentration fluctuations. Thus, there is no decay in the spectrum $E_C(k)$ at high wave numbers, rather, the fluctuation intensity piles up at larger wave numbers (cf. Fig. 5). Note, however, that the concentration variance (43) remains finite and small, relative to the average concentration C_0^2, throughout the computations (cf. Fig. 4).

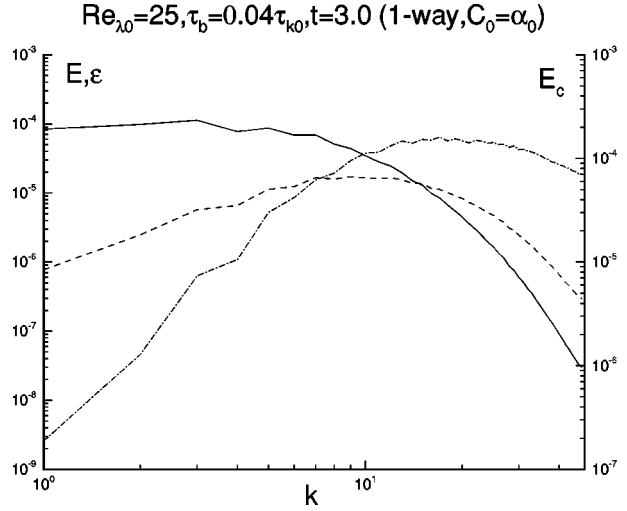

FIG. 5. Spectra of the turbulence kinetic energy $E(k)$ (solid curve), dissipation $\epsilon(k)$ (dashed curve), and bubble concentration fluctuations $E_c(k)$ (dash–dotted curve).

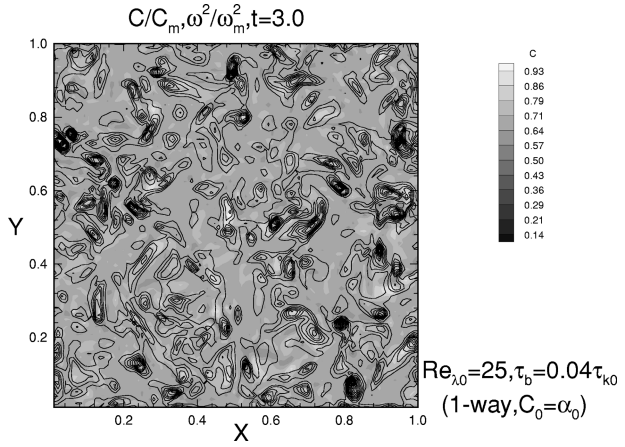

FIG. 6. Turbulence enstrophy and bubble concentration normalized by the maximum values.

Figure 6 shows the DNS results obtained at $t=3$ for the bubble concentration (gray scale) and flow enstrophy field (contour lines) in the (x,y) plane at $z=0.5$. Although the bubble response time is much smaller than the Kolmogorov time scale, we still observe the accumulation of bubbles in the zones of maximum enstrophy (corresponding to the centers of intense vortices). This means that even for such small τ_b the bubble inertia, owing to the added mass, influences the bubble motion, and causes the preferential accumulation of bubbles in the high-enstrophy regions of the flow and the initial growth of the concentration variance. Note that the time interval $\Delta t=2$ corresponds approximately to six characteristic vortex time scales, $\langle \omega^2\rangle^{-1/2}$, estimated as an average Kolmogorov time $\overline{\tau_k}$ for $1<t<3$, $\langle \omega^2\rangle^{-1/2}\sim \overline{\tau_k}\simeq 0.3$.

In order to quantify the accumulation effects we calculated the enstrophy-conditioned average bubble concentration, $\langle C\rangle_\omega$, and its variance, $\langle C'^2\rangle_\omega$, using the data shown in Fig. 6 and Eqs. (26) and (27) with the enstrophy increment $\Delta\omega^2=0.5$. Figure 7 shows the dependence of $\langle C\rangle_\omega$ and $\langle C'^2\rangle_\omega$ on ω^2. As in the case of bubble dispersion in the TG vortex discussed earlier, both $\langle C\rangle_\omega$ and $\langle C'^2\rangle_\omega$ increase in the high-enstrophy regions of the flow. However, since the bubble response time is much smaller than the Kolmogorov time scale, the bubble preferential accumulation is significantly reduced compared to the TG-vortex case, where $\tau_b \simeq \tau_f$. Note also that fluctuations of both $\langle C\rangle_\omega$ and $\langle C'^2\rangle_\omega$ grow as the enstrophy increases, which shows the intermittent nature of the high-enstrophy regions in turbulence.

Now, we introduce a mathematical model to explain how the ratio τ_b/τ_k governs the preferential accumulation process and the growth of the local concentration gradients in isotropic turbulence.

Let us consider a single vortex with a radius of the order of the Kolmogorov length scale η and core vorticity $\omega_0=1/\tau_k$. Assume that the bubble response time is much smaller than the Kolmogorov time scale, $\tau_b/\tau_k \ll 1$. Then, the local accumulation rate can be estimated from the solu-

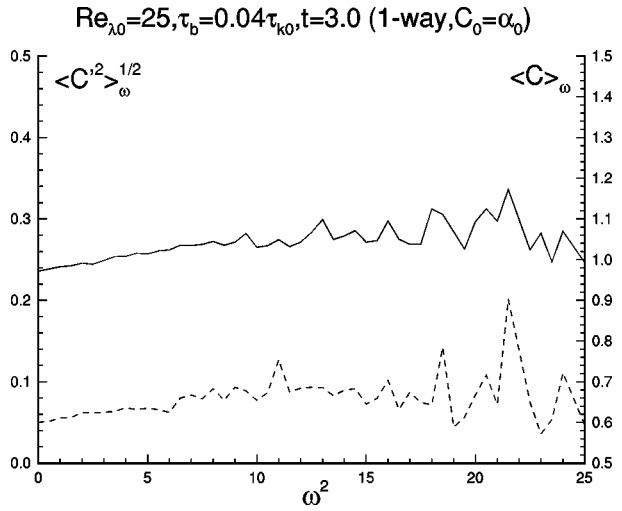

FIG. 7. Dependence of the enstrophy-conditioned average bubble concentration (solid curve) and its variance (dashed curve) on the enstrophy.

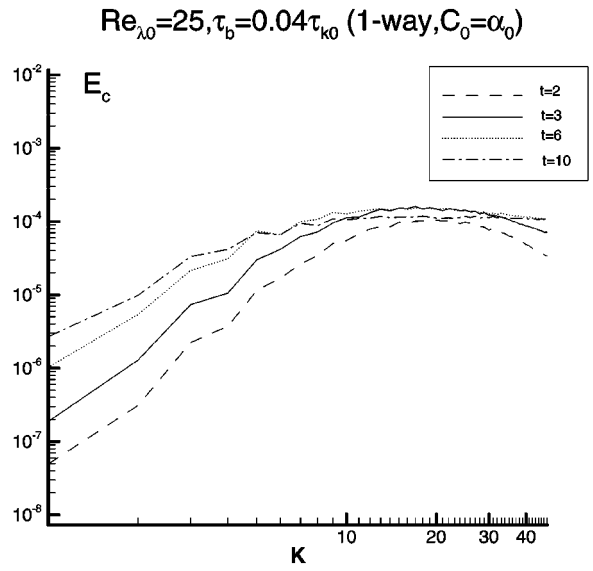

FIG. 8. Instantaneous spectra of the bubble concentration fluctuations $E_c(k)$ at four different times (with one-way coupling).

tion (33) for the bubbles concentration in the TG vortex as

$$\frac{\partial C/\partial t}{C_0} \simeq \tau_b \omega_0^2 \simeq \frac{\tau_b}{\tau_k^2}. \tag{44}$$

Thus the difference in bubble concentration between the inside and outside of the vortex, $\Delta C = C_i - C_o$, is related to (τ_b/τ_k) via

$$\frac{\Delta C}{C_o} \simeq \frac{\tau_b}{\tau_k}, \tag{45}$$

and the corresponding concentration gradient is

$$\frac{|\nabla C|}{C_o} \sim \frac{\Delta C}{C_o \eta} \sim \frac{\tau_b}{\eta \tau_k}. \tag{46}$$

The smoothness condition (34) is then rewritten in the form

$$\frac{|\nabla C|}{C_o} \Delta x \simeq \frac{\tau_b}{\tau_k} \frac{\Delta x}{\eta} \ll 1. \tag{47}$$

The relations (44) and (46) show that both the accumulation rate and the local concentration gradient are directly proportional to the ratio (τ_b/τ_k) for $\tau_b < \tau_k$.

Note that according to (45), the variance of the concentration fluctuations is proportional to the ratio $(\tau_b/\tau_k)^2$ that decreases with time in decaying turbulence, since the Kolmogorov time scale increases monotonically. This prediction agrees with our DNS results for $\langle C'^2 \rangle$ in Fig. 4, which shows that the concentration variance decays with time after the initial transient ($1 < t < 5$).

It should be noted that both the accumulation of bubbles and the absence of the diffusivity in the transport equation for the bubble concentration (17) may lead to instabilities in the numerical solution due to the development of steep gradients in the concentration field. The occurrence of this numerical instability depends on the initial distribution of the bubble concentration, the flow Reynolds number, and the bubble response time. In our DNS we chose the initial microscale Reynolds number $\mathrm{Re}_{\lambda 0} = 25$, so that at time of the injection of bubbles ($t = 1$) the small-scale motions are resolved, i.e., $k_{\max}\eta \geqslant 1$, where $k_{\max} = N_g \pi$ is the maximum wave number for the given grid resolution $N_g = 96$. The numerical instability may occur for higher-inertia bubbles, i.e., for τ_b of the order of the Kolmogorov time scale τ_k. However, prescribing $\tau_b \simeq \tau_k$ would violate the condition $d_b < \eta$, which is necessary for deriving Eq. (16) of bubble motion.

In our DNS we prescribe $\tau_b = 0.04\tau_{k0} = 0.006$ for which the bubble diameter ($d_b \simeq 3.47 \times 10^{-3}$) is smaller than the Kolmogorov length scale at the time of the bubble injection ($\eta \simeq 3.5 \times 10^{-3}$ at $t = 1$) (both d_b and η are dimensionless here), to remain within the validity limit of Eq. (16). No instability occurs in our DNS under these conditions for both cases of the initially uniform and the initially linear bubble concentration fields. This is evident in Fig. 8, which shows the instantaneous concentration variance spectra, obtained from our DNS for the initially uniform bubble distribution, at four different times. The time evolution of the concentration spectrum in Fig. 8 and the corresponding concentration variance, $\langle C'^2 \rangle$ (the dash–dotted curve in Fig. 4) show that no numerical instability occurs. The spectrum $E_C(k)$ at high wave numbers approaches an asymptotic form at $t = 10$ (Fig. 8). The high wave number range in the spectrum (i.e., $k \geqslant 40$) would detect any numerical instability if it existed. Furthermore, Fig. 4 shows that the concentration variance, $\langle C'^2 \rangle$, decays with time for $t > 5$.

The reason for the absence of the instability is that the fluctuations of the bubble concentration, caused by the preferential accumulation, are proportional to the ratio τ_b/τ_k that decreases with time (approximately as $\sim 1/t$) in decaying turbulence, as discussed above.

C. Two-way coupling effects on decaying turbulence

Here we examine the effects of the dispersed bubbles on the temporal development of decaying isotropic turbulence. We consider three cases with different initial bubble concen-

tration profiles in the z direction, but with the same bubble response time as in the one-way coupling case.

The first case is for a uniform initial bubble concentration,

$$C_0=\alpha_0, \tag{48}$$

where α_0 is a reference concentration set equal to 0.005 to allow neglecting bubble–bubble interactions.

The second case is for stable linear stratification, with a constant concentration gradient in the vertical (z) coordinate,

$$C_0=\alpha_0(1+z), \tag{49}$$

while the third case is for unstable linear stratification,

$$C_0=\alpha_0(2-z). \tag{50}$$

In the cases of stable and unstable stratification, periodic boundary conditions in the z direction are imposed on the instantaneous concentration fluctuation $C'=C-\langle C\rangle$.

We first consider the modification of the turbulence energy spectrum. We define a band-averaged kinetic energy spectrum $E(k)$ as

$$E(k)=\frac{1}{2}\sum_{k<|\mathbf{k}|<k+1}|\boldsymbol{U}(\mathbf{k})|^2. \tag{51}$$

Performing the Fourier transform of the fluid momentum equation (14) and using the incompressibility condition for the fluid velocity $[k_\beta U_\beta(\mathbf{k})=0]$ we obtain

$$\partial_t E(k)=T(k)-\epsilon(k)+\Psi_b(k), \tag{52}$$

where dissipation $\epsilon(k)$ is

$$\epsilon(k)=2\nu k^2 E(k), \tag{53}$$

and the band-averaged spectral energy transfer function $T(k)$ is

$$T(k)=\sum_{k<|\mathbf{k}|<k+1}T(\mathbf{k}), \tag{54}$$

$$T(\mathbf{k})=\mathrm{Im}\left(k_m\sum_{\mathbf{k}'}U_n(\mathbf{k}')U_m(\mathbf{k}-\mathbf{k}')U_n^*(\mathbf{k})\right). \tag{55}$$

The source of the modification of the energy spectrum and spectral transfer process is $\Psi_b(k)$, which can be regarded as a spectral buoyancy flux, analogous to that in a stratified fluid with density C', and is defined as

$$\Psi_b(k)=\sum_{k<|\mathbf{k}|<k+1}\Psi_b(\mathbf{k}), \tag{56}$$

$$\Psi_b(\mathbf{k})=g\ \mathrm{Re}[C'(\mathbf{k})U_z^*(\mathbf{k})]. \tag{57}$$

Figure 9 shows the difference between the energy spectra in two-way and one-way coupling cases computed at time $t=3$. As expected, the turbulence energy increases in the case of unstable stratification and is reduced in the case of stable stratification. In the nonstratified two-way coupling case, the spectrum remains practically unchanged compared to the one-way coupling case. Figure 10 shows the corresponding modification of the dissipation function $\epsilon(k)$.

Figure 11 shows the effect of bubbles on the turbulence energy transfer function $T(k)$ in the three test cases. In the case of stable stratification, the transfer of energy from lower to higher wave numbers is reduced (since the difference $T_{2w}-T_{1w}$ is positive) compared to the one-way coupling case, owing to the bubble-induced buoyancy. On the other hand, in the case of unstable stratification, the transfer of energy from low to high k is enhanced (i.e., the difference $T_{2w}-T_{1w}$ is negative). In the nonstratified case, the two-way coupling does not affect $T(k)$.

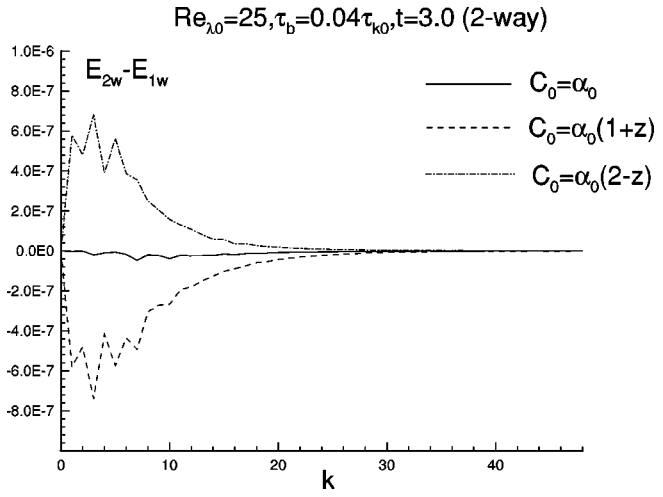

FIG. 9. Modification of the turbulence kinetic energy spectrum in a bubble-laden decaying turbulence.

The source terms $\Psi_b(k)$, or spectral buoyancy fluxes, in the three cases are shown in Fig. 12. Comparing it with Fig. 11 for the modification of the energy transfer function, we find that spectral peaks of both $\Psi_b(k)$ and $(T_{2w}-T_{1w})$ [of the order $O(10^{-7})$] are located in the wave number range $0<k<10$. Consequently, the peaks of the energy spectra differences $(E_{2w}-E_{1w})$ are of the order $O(10^{-7})$ and are located in the same wave number range (cf. Fig. 9 and Figs. 11 and 12).

Figure 13 shows the difference between the kinetic energy spectra of the bubble phase and the fluid $[E_b(k)-E(k)]$. In all cases the bubble kinetic energy $E_b(k)$

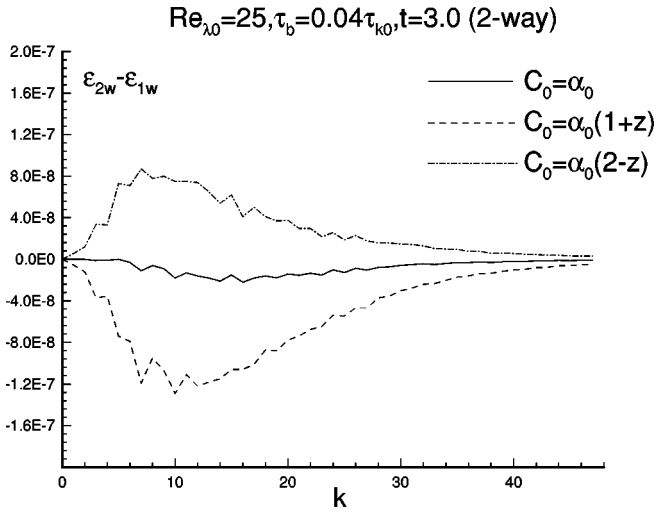

FIG. 10. Modification of the turbulence dissipation spectrum.

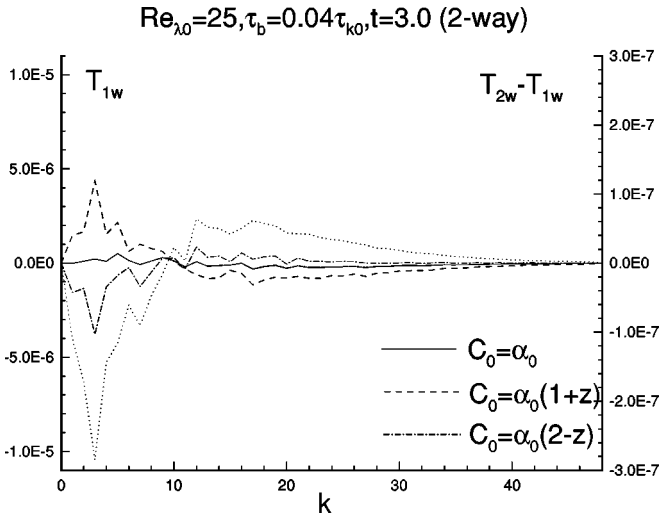

FIG. 11. Modification of the spectral energy transfer function. The energy transfer function in the one-way coupling case, $T_{1w}(k)$, is shown by the dotted curve.

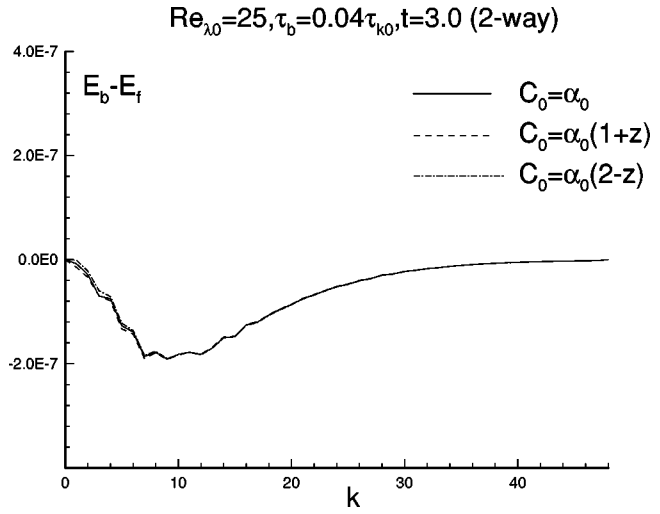

FIG. 13. The difference between the bubble and fluid kinetic energy spectra.

is reduced in the small-k region of the spectrum compared to $E(k)$ due to the bubble inertia (i.e., owing to the added-mass inertia). However, since the bubble response time is much smaller than the Kolmogorov scale, the observed difference is only of the order of 1% of the energy peak $E_{\max}(k)\simeq 10^{-4}$ (cf. Fig. 5).

The transport equation for the turbulence kinetic energy, $E(t)=\frac{1}{2}|\mathbf{U}(\mathbf{r},t)|^2$, can be obtained either from Eq. (52) by integrating over k, or directly from Eq. (14) for the fluid momentum by ensemble averaging, in the form

$$\partial_t E = -\epsilon + g\langle C' U_z\rangle. \tag{58}$$

Equation (58) shows that the modification of $E(t)$ is caused by the buoyancy flux term, $g\langle C' U_z\rangle$. We evaluate this term from our DNS results as an average over a horizontal plane (x,y) for each z. Figure 14 shows the dependence of $\langle C' U_z\rangle/C_0$ on the z coordinate. We find that the buoyancy flux is nearly constant of value zero in the nonstratified case, and nearly uniform negative and positive in the cases of stable and unstable stratification, respectively. These results suggest a closure model for the correlation $\langle C' U_z\rangle$ in the form

$$\langle C' U_z\rangle = -D_z \frac{\partial}{\partial z}\langle C\rangle, \tag{59}$$

with a uniform diffusivity coefficient D_z.

Figure 15 shows the time development of the turbulence kinetic energy relative difference $(E_{2w}-E_{1w})/E_{1w}$ due to the two-way coupling. As expected, $E_{2w}(t)$ is reduced compared to $E_{1w}(t)$ in the case of stable stratification, and increased for unstable stratification. In the nonstratified case, the modification of $E(t)$ compared to the one-way coupling case is negligible.

Therefore, two-way coupling enhances or reduces the turbulence decay rate depending on whether the stratification (due to the bubbles) is stable or unstable, while in the nonstratified case there is no influence of the bubbles on the turbulence dynamics.

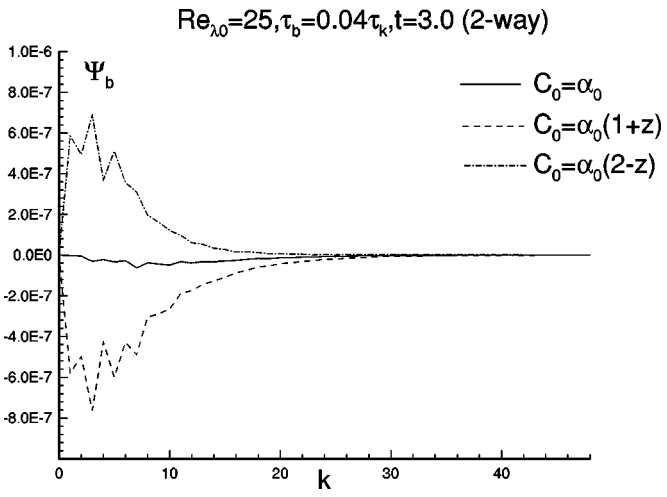

FIG. 12. Spectral buoyancy flux $\Phi_b(k)$.

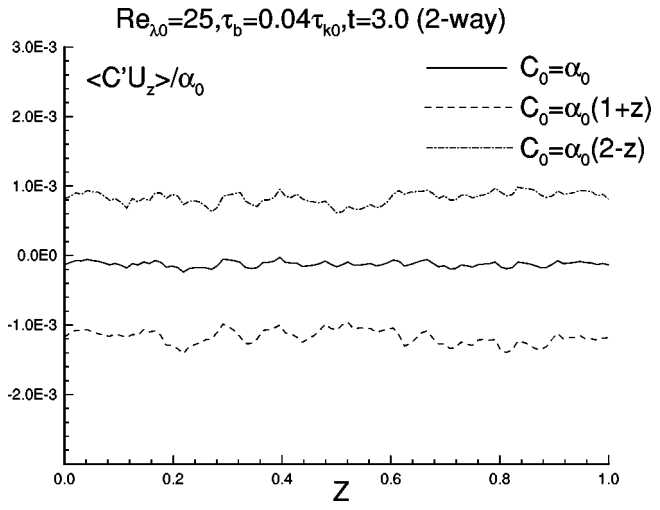

FIG. 14. Dependence of the normalized buoyancy flux, $\langle C' U_z\rangle/\alpha_0$, averaged over horizontal (z) planes, on the z coordinate.

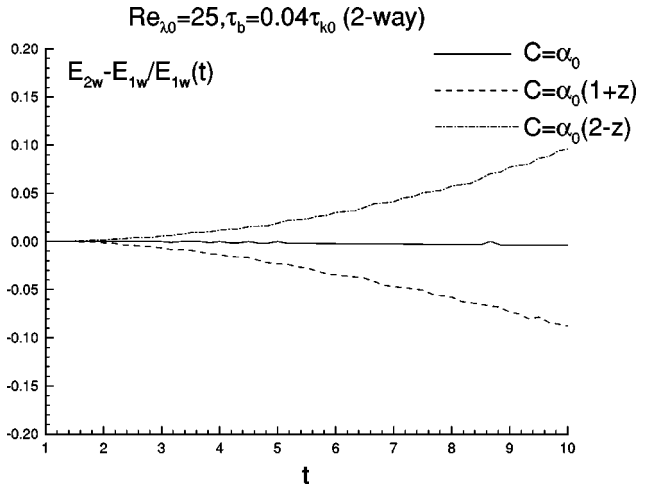

FIG. 15. Time development of the turbulence kinetic energy modification.

IV. CONCLUDING REMARKS

We have performed direct numerical simulations (DNS) of bubble-laden isotropic decaying turbulence using the two-fluid approach (TF) instead of the Eulerian–Lagrangian approach (EL). The motivation for this study is that EL requires considerable computational resources, especially for the case of two-way coupling, where the instantaneous trajectories of a large number of individual bubbles need to be computed.

We developed the TF formulation by spatially averaging the instantaneous equations of the carrier flow and bubble phase over a scale of the order of the Kolmogorov length scale, which, in our case, is much larger than the bubble diameter. On that scale, the bubbles are treated as a continuum (without molecular diffusivity) characterized by the bubble phase velocity field and concentration (volume fraction). The bubble concentration, C, is assumed small enough ($C \leqslant 10^{-3}$) to neglect the bubble–bubble interactions.

As a test case, we performed direct simulation of a bubble-laden Taylor–Green vortex with one-way coupling and a bubble response time of the order of the flow time scale (the inverse of the mean vorticity). This simple flow allows a direct examination of the effects of the preferential accumulation of bubbles in the high-enstrophy regions of the flow on the accuracy of the two-fluid formulation. The temporal development of the maximum bubble concentration obtained from DNS agrees well with the analytical solution.

DNS of the bubble-laden decaying turbulence were also performed for both cases of one-way and two-way coupling. Here, the bubble diameter and response time are much smaller than the Kolmogorov length and time scales, respectively. In this case, as expected, the effects of the preferential accumulation of the bubbles are not pronounced. The results show that the bubble-laden flow is analogous to a stratified flow with an effective density $= (1-C)\rho_f$. Thus, due to the two-way interaction, the turbulence decay is enhanced with stable stratification, and reduced with unstable stratification.

The results show that the TF approach can be successfully implemented in the DNS of turbulent flows laden with microbubbles. It should be noted that the results discussed above are obtained for comparatively low Reynolds numbers and smooth initial bubble distribution to ensure a sufficient resolution of the fluid and bubble velocity and concentration fields. In a recently completed study[29] we examined a decaying isotropic turbulence laden with solid heavy particles with a response time much smaller than the Kolmogorov time scale of the turbulence. In this case, the TF formulation is analogous to the ''dusty gas'' formulation.[27,28]

ACKNOWLEDGMENTS

This work was supported by ONR Grant No. N00014-96-1-0213 administered by Dr. Edwin Rood. The computations were performed on Cray C98 located at the Naval Oceanographic Center, Mississippi.

APPENDIX: EQUATION OF MOTION OF A SINGLE BUBBLE IN A NONUNIFORM FLOW

Consider a spherical bubble of radius $a=d/2$ and density ρ_b located at $\mathbf{x}_b(t)$ and moving with velocity,

$$V_i(t)=\frac{dx_i}{dt}, \tag{A1}$$

in a nonuniform fluid flow $U_i(r,t)$. The equation for the bubble velocity is

$$m_b\frac{dV_i}{dt}=m_b g_i+\oint_{S_b} dS n_j(-P\delta_{ij}+\sigma_{ij}), \tag{A2}$$

where $m_b=4/3\pi a^3\rho_b$ is the mass of the bubble, d/dt is the material derivative along the bubble trajectory, g_i is the acceleration due to gravity, and the integral is taken over the bubble surface S_b, where $|r-x_b|=a$. The viscous stresses tensor σ_{ij} is defined as

$$\sigma_{ij}=\mu\left(\frac{\partial U_i}{\partial x_j}+\frac{\partial U_j}{\partial x_i}\right), \tag{A3}$$

where μ is the dynamic viscosity of the fluid.

The pressure field P and the fluid velocity field U in (A2) and (A3) are generally obtained from the boundary problem, formulated for a given flow at infinity (i.e., the undisturbed flow) and proper boundary conditions at the bubble surface. For a small bubble in liquid water, the boundary conditions generally are well approximated by the no-slip conditions for the fluid velocity.[10–12] Thus, the corresponding equations are formulated as

$$\rho_f(\partial_t U_i+U_j\partial_j U_i)=-\partial_i P+\mu\partial^2 U_i+\rho_f g_i, \tag{A4}$$

$$\partial_j U_j=0, \tag{A5}$$

where $\partial_j\equiv\partial/\partial x_j$. The boundary conditions are

$$\begin{aligned} &U_i(r,t)\big|_{|r-x_b|\gg a}=U_i^0(r,t),\\ &U_i(r,t)\big|_{|r-x_b|=a}=V_i(t), \end{aligned} \tag{A6}$$

where $U_i^0(r,t)$ is the undisturbed fluid velocity sufficiently far from the bubble surface.

It is convenient to represent the fluid velocity U_i as a sum of the undisturbed velocity, U_i^0, and a disturbance velocity, U_i^d, brought about by the bubble,

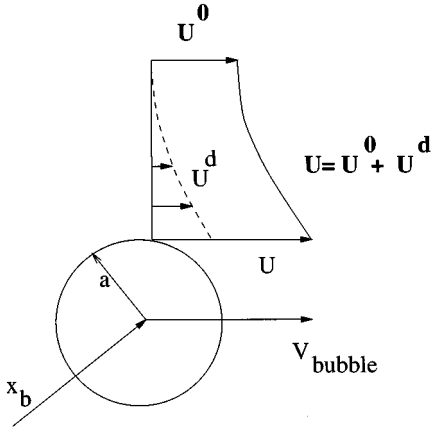

FIG. 16. Flow decomposition in the vicinity of a bubble surface.

$$U_i(r,t)=U_i^0(r,t)+U_i^d(r,t). \tag{A7}$$

Figure 16 shows the decomposition of the flow (A7) in the vicinity of the bubble surface for a case of rectilinear motion (i.e., where the bubble and undisturbed fluid velocities, $\mathbf{V}$ and $\mathbf{U}^0$, are parallel).

The undisturbed fluid velocity, U_i^0, satisfies the Navier–Stokes equations,

$$\rho_f\frac{DU_i^0}{Dt}=-\partial_i P^0+\mu\partial^2 U_i^0+\rho_f g_i, \tag{A8}$$

$$\partial_j U_j^0=0, \tag{A9}$$

where

$$D/Dt=\partial_t+U_j^0\partial_j. \tag{A10}$$

From Eqs. (A4), (A5), and (A6) we obtain the following equations for the disturbance velocity, U_i^d,

$$\rho_f\left(\frac{DU_i^d}{Dt}+U_j^d\partial_j U_i^0+U_j^d\partial_j U_i^d\right)=-\partial_i P^d+\mu\partial^2 U_i^d, \tag{A11}$$

$$\partial_j U_j^d=0, \tag{A12}$$

with boundary conditions

$$\begin{aligned} &U_i^d(r,t)\big|_{|r-x_b|\gg a}=0,\\ &U_i^d(r,t)\big|_{|r-x_b|=a}=V_i(t)-U_i^0[x_b(t),t]. \end{aligned} \tag{A13}$$

Note that the gravity term is included only in Eq. (A8) for the undisturbed flow since it does not depend on the velocity field. The second and third terms on the lhs of Eq. (A11) are due to the fact that the material derivative D/Dt is defined in (A10) with respect to the undisturbed flow U_i^0. Adding the lhs of both (A8) and (A11) produces the lhs of (A4).

Now we can rewrite the integral on the rhs of (A2) as a sum of two parts:

$$\begin{aligned} \oint_{S_b} dSn_j(-P\delta_{ij}+\sigma_{ij})=&\oint_{S_b} dSn_j(-P^0\delta_{ij}+\sigma_{ij}^0)\\ &+\oint_{S_b} dSn_j(-P^d\delta_{ij}+\sigma_{ij}^d), \end{aligned} \tag{A14}$$

where

$$\sigma_{ij}^d\equiv\mu(\partial_j U_i^d+\partial_i U_j^d).$$

The first integral term on the rhs of (A14) is the contribution from the undisturbed flow, U^0, and the second term is the contribution of the disturbance field, U^d.

The contribution from the undisturbed flow can be calculated explicitly for the case of the bubble with a radius much smaller than the characteristic length scale of the flow. Accordingly, the variations of U^0 and P^0 inside the bubble volume can be neglected and the integral on the rhs of (A14) can be rewritten with the use of Gauss theorem as

$$\begin{aligned} \oint_{S_b} dSn_j(-P^0\delta_{ij}+\sigma_{ij}^0)&=\int_{\mathrm{Vol}_b}(-\partial_i P^0+\mu\partial^2 U_i^0)dV\\ &\simeq \mathrm{Vol}_b\ F_i^0, \end{aligned} \tag{A15}$$

where the bubble volume $\mathrm{Vol}_b=4/3\pi a^3$ and the force F_i^0 is [cf. Eq. (A8)]

$$F_i^0\equiv-\partial_i P^0+\mu\partial^2 U_i^0=\rho_f\left(\frac{DU_i^0}{Dt}-g_i\right). \tag{A16}$$

The contribution of the disturbance field can be redefined as

$$\oint_{S_b} dSn_j(-P^d\delta_{ij}+\sigma_{ij}^d)=\mathrm{Vol}_b\ F_i^d. \tag{A17}$$

Assuming that the density of the bubble gas negligible compared to that of the surrounding fluid, the equation for the bubble motion (A2) reduces to[26,6,7]

$$0=F_i^0+F_i^d. \tag{A18}$$

The force F_i^d, caused by the disturbance, is defined by Eq. (A17) for the velocity and pressure fields U^d and P^d obtained from the solution of the equations (A11)–(A13) for the disturbance flow. It is clear that the bubble motion [(A1) or (A2)] is coupled with the dynamics of the undisturbed flow, U^0, P^0, defined by Eqs. (A8) and (A9). Once the problem (A11)–(A13) for the disturbance field is solved, the equation of the bubble motion is fully defined in terms of the flow U^0.

In general, the disturbance flow represented by (A11)–(A13) has no analytical solution and can be obtained only via a numerical solution of the 3-D time-dependent equations. However, in the case of a sufficiently small bubble, for which the inertia terms on the lhs of (A11) are negligible, the problem is reduced to the unsteady Stokes problem:[17]

$$\rho_f\frac{\partial U_i^d}{\partial t}=-\partial_i P^d+\mu\partial^2 U_i^d, \tag{A19}$$

$$\partial_j U_j^d=0, \tag{A20}$$

with the boundary conditions (A13). Then, the expression for the force caused by the disturbance is given by Maxey and Riley[17] in the form

$$F_i^d = \frac{9\mu}{2a^2}(U_i - V_i) + \frac{\rho_f}{2}\left(\frac{DU_i}{Dt} - \frac{dV_i}{dt}\right). \tag{A21}$$

The first and second terms in (A21) correspond to the Stokes drag and added-mass forces, respectively. The contributions due to the Basset and lift forces can be neglected in the considered case of small bubbles.[17,18]

[1]C. T. Crowe, T. R. Troutt, and J. N. Chung, ''Numerical models for two-phase turbulent flows,'' Annu. Rev. Fluid Mech. **28**, 11 (1996).
[2]S. E. Elghobashi, ''On predicting particle-laden turbulent flows,'' Appl. Sci. Res. **52**, 309 (1994).
[3]S. E. Elghobashi and T. W. Abou-Arab, ''A two-equation turbulence model for two-phase flows,'' Phys. Fluids **26**, 931 (1983).
[4]J. K. Eaton and J. R. Fessler, ''Preferential concentration of particles by turbulence,'' Int. J. Multiphase Flow Suppl. **20**, 169 (1994).
[5]L.-P. Wang and M. R. Maxey, ''Settling velocity and concentration distribution of heavy particles in homogeneous isotropic turbulence,'' J. Fluid Mech. **256**, 27 (1993).
[6]P. M. Rightley, ''Bubble dispersion and interphase coupling in a free shear flow,'' Ph.D. thesis, University of California, San Diego, 1995.
[7]P. M. Rightley and J. C. Lasheras, ''Bubble dispersion and interphase coupling in a free shear flow,'' J. Fluid Mech. (in press).
[8]D. A. Drew, ''Mathematical modeling of two-phase flow,'' Annu. Rev. Fluid Mech. **15**, 261 (1983).
[9]D. Z. Zhang and A. Prosperetti, ''Momentum and energy equations for disperse two-phase flows and their closure for dilute suspensions,'' Int. J. Multiphase Flow **23**, 425 (1997).
[10]V. G. Levich, *Physicochemical Hydrodynamics* (Prentice–Hall, Englewood Cliffs, NJ, 1962), p. 432.
[11]G. K. Batchelor *An Introduction to Fluid Mechanics* (Cambridge Univ. Press, 1967), p. 257.
[12]H. Clift, J. R. Grace, and M. E. Weber, *Bubbles, Drops and Particles* (Academic, New York, 1978).
[13]R. M. Detsch, ''Small air bubbles in reagent grade water and seawater: 1. Rise velocities of 20- to 1000-μm diameter bubbles,'' J. Geophys. Res. **96**, 8901 (1991).
[14]R. Mei, C. J. Lawrence, and R. J. Adrian, ''Unsteady drag on a sphere at finite Reynolds number with small fluctuations in the free-stream velocity,'' J. Fluid Mech. **233**, 613 (1991).
[15]C. J. Lawrence and R. Mei, ''Long-time behaviour of the drag on a body in impulsive motion,'' J. Fluid Mech. **283**, 307 (1995).
[16]G. Sridhar and J. Katz, ''Drag and lift forces on microscopic bubbles entrained by a vortex,'' Phys. Fluids **7**, 389 (1995).
[17]M. R. Maxey and J. J. Riley, ''Equation of motion for a small rigid sphere in a non-uniform flow,'' Phys. Fluids **197**, 883 (1983).
[18]G. R. Ruetsch and E. Meiburg, ''Two-way coupling in shear layers with dilute bubble concentrations,'' Phys. Fluids **6**, 2656 (1994).
[19]S. E. Elghobashi and G. C. Truesdell, ''On the two-way interaction between homogeneous turbulence and dispersed solid particles. I: Turbulence modification,'' Phys. Fluids A **5**, 1790 (1993).
[20]T. Gerz, U. Schumann, and S. Elghobashi, ''Direct simulation of stably stratified homogeneous turbulent shear flows,'' J. Fluid Mech. **200**, 563 (1989).
[21]U. Schumann, ''Realizability of Reynolds-stress turbulence models,'' Phys. Fluids **20**, 721 (1977).
[22]G. I. Taylor, ''On the decay of vortices in a viscous fluid,'' Philos. Mag. **XLVI**, 671 (1923).
[23]L.-P. Wang and M. R. Maxey, ''The motion of microbubbles in a forced isotropic and homogeneous turbulence,'' Appl. Sci. Res. **51**, 291 (1993).
[24]M. R. Maxey, E. J. Chang, and L.-P. Wang, ''Simulation of interactions between microbubbles and turbulent flows,'' Appl. Mech. Rev. **4**, S70 (1994).
[25]M. R. Maxey, ''The gravitational settling of aerosol particles in homogeneous turbulence and random flow fields,'' J. Fluid Mech. **174**, 441 (1987).
[26]O. A. Druzhinin, ''On the two-way interaction in two-dimensional particle-laden flows: The accumulation of particles and flow modification,'' J. Fluid Mech. **297**, 49 (1995).
[27]P. G. Saffman, ''On the stability of laminar flow of a dusty gas,'' J. Fluid Mech. **13**, 120 (1962).
[28]F. E. Marble, ''Dynamics of dusty gases,'' Annu. Rev. Fluid Mech. **2**, 397 (1970).
[29]O. A. Druzhinin and S. E. Elghobashi, ''DNS of particle-laden turbulent flows using the two-fluid approach,'' in preparation.